Journal of Hazardous Materials 209–210 (2012) 467–477

Contents lists available at SciVerse ScienceDirect

Journal of Hazardous Materials

journal homepage: www.elsevier.com/locate/jhazmat

Adsorption of heavy metal ions using hierarchical $CaCO_3$–maltose meso/macroporous hybrid materials: Adsorption isotherms and kinetic studies

Xiaoming Ma*, Liping Li, Lin Yang, Caiyun Su, Kui Wang, Shibao Yuan, Jianguo Zhou

College of Chemistry and Environmental Science, Henan Normal University, Key Laboratory of Green Chemical Media and Reactions, Ministry of Education, Xinxiang 453007, PR China

ARTICLE INFO

Article history:
Received 16 November 2011
Received in revised form 13 January 2012
Accepted 16 January 2012
Available online 23 January 2012

Keywords:
Hierarchical meso/macroporous structure
Hybrid materials
Heavy metal ions
Calcium carbonate–maltose
Adsorption isotherm
Kinetics

ABSTRACT

Highly ordered hierarchical calcium carbonate is an important phase and has technological interest in the development of functional materials. The work describes hierarchical $CaCO_3$–maltose meso/macroporous hybrid materials were synthesized using a simple gas-diffusion method. The uniform hexagonal-shaped $CaCO_3$–maltose hybrid materials are formed by the hierarchical assembly of nanoparticles. The pore structure analysis indicates that the sample possesses the macroporous structure of mesoporous framework. The distinguishing features of the hierarchical $CaCO_3$–maltose materials in water treatment involve not only high removal capacities, but also decontamination of trace metal ions. Langmuir model fitted the equilibrium data better than the Freundlich isotherm. The maximum removal capacity of the $CaCO_3$–maltose hybrid materials for Pb^{2+}, Cd^{2+}, Cu^{2+}, Co^{2+}, Mn^{2+} and Ni^{2+} ions was 3242.48, 487.80, 628.93, 393.70, 558.66 and 769.23 mg/g, respectively. Adsorption data were modeled using the pseudo-first-order, pseudo-second-order and intra-particle diffusion kinetics equations. The results indicate that pseudo-second-order kinetic equation and intra-particle diffusion model can better describe the adsorption kinetics. The adsorption and precipitation transformation mechanism can be considered due to hierarchical meso/macroporous structure, rich organic ligands of the $CaCO_3$–maltose hybrid materials and the larger solubility product of $CaCO_3$.

1. Introduction

The contamination of freshwater has become one of the main threats to the normal life of human [1]. Heavy metals, such as lead and cadmium, because of toxicity, are harmful to living organism [2–4]. To decontaminate the water polluted by heavy metals, various treatment technologies have been tried and used, including chemical precipitation, solvent extraction, adsorption, etc. In these technologies, adsorption seems to be the most convenient method and is often the method of choice. However, economy and efficiency have largely hampered the commercial applications of some adsorbents. Therefore, the high efficiency and inexpensive adsorptive materials are still demanded.

The porous materials, as adsorbents, have attracted tremendous research interest and have been put into practice [5–8]. Especially, the chemically designed inorganic–organic hybrid materials with porous structures have attracted considerable attention because of the combination of properties with respect to the inorganic and the organic components, which allows to tailor density, chemical reactivity, and thermal stability [9–14]. Compared with single-sized porous materials, the materials with hierarchical meso/macroporous structure as adsorbents can enhance properties due to increased mass transport through the large pore channels of the materials and maintenance of a specific surface area on the level of fine pore systems [15–20]. However, the fabrication of inorganic–organic hybrid materials with hierarchical meso/macroporous structure, which have more advantages on adsorption, is till a challenge as regards their application potential.

Carbonate minerals are effective in removing heavy metals and the mechanism of adsorption was suggested to be ion-exchange and precipitation on the carbonate surface [21–23]. It is well known that calcium carbonate is one of the cheapest materials in nature and harmless to humans. Furthermore, the larger solubility product of $CaCO_3$ could be lead to precipitation transformation happened between $CaCO_3$ and some carbonates, which could increase greatly the adsorption capacity of the metal ions. Although calcium carbonate has been studied for removal of heavy metal ions [22,24–26], the low efficiency and further treatment necessity for the sludge significantly limit the practical applications in water treatment. Otherwise, maltose is one of the predominant saccharide and has many hydroxyl groups, which could interact with heavy metal ions. The interaction makes it possible to remove the heavy metal ions from the waste water.

Herein, our aim is to facilely synthesize the inorganic–organic $CaCO_3$–maltose hybrid materials with hierarchical meso/macroporous structure, which could be the high efficiency and inexpensive adsorbents in removal of heavy metal ions from waste water. The maximum removal capacities for Pb^{2+},

* Corresponding author. Tel.: +86 373 3325058; fax: +86 373 3328507.
E-mail address: sunshinyma@hotmail.com (X. Ma).

0304-3894/$ – see front matter © 2012 Elsevier B.V. All rights reserved.
doi:10.1016/j.jhazmat.2012.01.054

Cd^{2+}, Cu^{2+}, Co^{2+}, Mn^{2+} and Ni^{2+} ions were higher than the reported previously. The adsorption and precipitation transformation mechanism can be considered due to rich organic ligands of the $CaCO_3$–maltose hybrid materials and the larger solubility product of $CaCO_3$. From these results, the $CaCO_3$–maltose hybrid materials with hierarchical meso/macroporous structure could be an alternative and efficiency absorbent for removal heavy metal ions.

2. Materials and methods

2.1. Materials

All chemicals used in the study are of analytical grade and were used without further purification. The corresponding metal nitrates were employed as the metal ions sources. Anhydrous calcium chloride and ammonium bicarbonate were purchased from Chemical Reagent Company of Tianjin. Maltose was purchased from Xiamen Sanland Chemicals Company Limited, China. Double distilled water was also used in our experiment. All glassware were soaked in a mixing K_2CrO_7/H_2SO_4 solution, then rinsed with double distilled water, and finally dried by the gas drier.

2.2. Preparation of the $CaCO_3$–maltose hybrid materials with hierarchical meso/macroporous structure

The experiments were carried out in a closed desiccator through a simple gas-diffused method at room temperature $25 \pm 1\,^{\circ}C$ with ammonium bicarbonate as the source of CO_2. First, the aqueous solution of $CaCl_2$ 0.05 M was freshly prepared. Maltose in a desired quantity was added to the $CaCl_2$ solution and stirred to ensure complete dissolution to obtain the mixed solution. Then, 20 mL mixed solution were added into a baker within a desiccator. Finally, the ammonium bicarbonate powder, which can decompose and release CO_2, was placed at the bottom of the desiccator. Then the two reactions:

$$CO_2 + H_2O \rightarrow {CO_3}^{2-} + 2H^+$$

$$Ca^{2+} + {CO_3}^{2-} \rightarrow CaCO_3$$

After 24 h the products were collected by centrifugation, washed with the double distilled water and anhydrous alcohol, and then dried at room temperature. The power products were obtained.

2.3. Adsorption equilibrium experiments

Solutions containing different concentrations of heavy metal ions were prepared. As-prepared $CaCO_3$ was added to the heavy metals solution under stirring. At different time intervals, the solids and liquids were separated by centrifugation and the concentrations of the heavy metals ions remaining in the solution were measured by atomic absorption spectroscopy. The amount of the heavy metal ions at equilibrium q_e (mg/g) on the adsorbent samples were calculated from the following equation:

$$q_e = \frac{(C_0 - C_e)V}{W} \quad (1)$$

where C_0 and C_e (mg/L) are the liquid phase concentrations of heavy metal ions at initial and equilibrium, respectively, V is the volume of the solution (L) and W is the mass of adsorbent used (g).

2.3.1. Effect of contact time

An as-prepared sample dose of 4 mg was added to 7 mL metal solution, with constant metal ion concentration. After different time interval (from 30 min to 2 h), the samples were taken out of the mixed solution.

2.3.2. Effect of pH

In order to study the influence of pH on the removal efficiency, NaAc–HAc buffer solutions was used to adjust and control the pH of the initial heavy metals solution. 4 mg products were added to 7 mL metal ions solution and the mixture was shaken on a thermostatic reciprocating shaker for 2 h with different pH from 3 to 8.

2.3.3. Effect of initial metal ions concentration

Effects of initial metal ions concentration on the adsorption of heavy metal ions were studied.

2.4. Adsorption kinetic experiments

The adsorption kinetic experiments were identical to those of isotherm experiments. The aqueous samples were taken to preset time intervals and the concentrations of heavy metal ions were similarly measured. The amount of adsorption at time t, q_t (mg/g), was calculated by:

$$q_t = \frac{(C_0 - C_t)V}{W} \quad (2)$$

where C_0 and C_t (mg/L) are the liquid phase concentrations of heavy metal ions at initial and any time t, respectively, V is the volume of the solution (L) and W is the mass of adsorbent (g).

2.5. Characterization

X-ray powder diffraction measurements were performed on a Bruker D & Advance X-ray powder diffractometer with graphite monochromatized CuKa (l = 0.15406 nm). A scanning rate of 0.05°/s was applied to record the pattern in the 2θ range of 10–70°. The morphology of nanoparticle self-assembly was observed by means of an AMARY-1000B (Germany Bruker) scanning electron microscope. HRTEM investigations were conducted on a JEOL JEL-2010 transmission electron microscope. N_2 adsorption–desorption isotherms were recorded on a Quantachrome NOVA 2000e sorption analyzer at liquid nitrogen temperature (77 K). The samples were degassed at 180 °C overnight prior to the measurement. The surface area was obtained by the Brunauer–Emmett–Teller (BET) method, and the pore size distribution was calculated from the adsorption branch of the isotherms by both the Barret–Joyner–Halenda (BJH) model. Thermogravimetry-differential thermal analysis (TG-DTA) of the samples was conducted on a Rigaku Standard Model thermal analyzer in air atmosphere with a heating rate of 10 °C/min. The concentration of heavy metal ions in the aqueous solution was analyzed by PerkinElmer Analyst 700 model atomic absorption spectroscopy (AAS) equipped with MHS 15 HGAAS system.

3. Results and discussion

3.1. Material characterizations

Fig. 1 shows the representative SEM and TEM images of the samples. It indicates that the hexagonal plates-shaped $CaCO_3$ (10–15 μm in diameter) is composed of the small granular micro-aggregates (see Fig. 1a and b). As a result of the aggregation of these micro-aggregates, the disordered wormhole-like macropores with diameter distribution of 200–500 nm are formed in the hybrid materials (Fig. 1c). As Fig. 1d shown, it reveals that the granular micro-aggregates consist of the smaller nanoparticles with the size of 5–10 nm. And it was the aggregation of these nanoparticles which results in the formation of the mesoporous in the hybrid materials. The well-defined mesoporous structure was further confirmed by TEM and HRTEM observation. Fig. 2a shows the TEM image of the hybrid materials and the obvious contrast between the dark edge and pale center is the evidence for their porous nature.

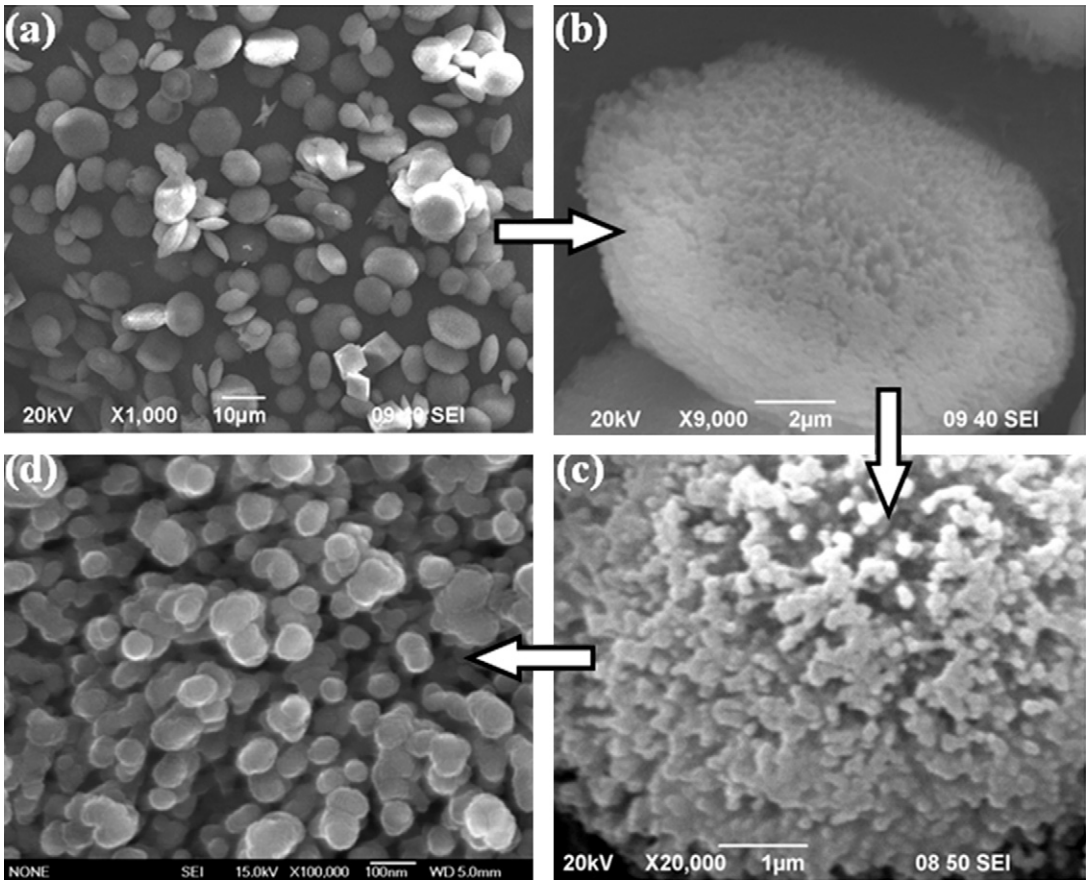

Fig. 1. The typical SEM images of the obtained $CaCO_3$–maltose hybrid materials.

From the HRTEM image (Fig. 2b), it can be observed that the regions of light contrast between individual nanocrystalline (as the black arrow shown) indicate the presence of interstices with the diameter of 5–10 nm within these particles.

In fact, the genesis of such a hierarchical meso/macroporous structure of $CaCO_3$ corresponds to a self-assembly formation mechanism, in which the maltose not only takes a role in the formation of the macroporous structure but also influences the textural properties and porosity of the hybrid materials. The possible formation mechanism of the $CaCO_3$ with hierarchical meso/macroporous structure is shown in Fig. 3. Firstly, after the maltose was added into $CaCl_2$ solution, calcium ions coordinated with some groups (such as —OH and —CO) of maltose [27–31] and the nanoparticles with size of about 5–10 nm were obtained. Secondly, under the mediation of maltose additive, self-assembly of these $CaCO_3$ nanoparticles precursors would result in the formation of the micro-aggregates and the mesoporous can be obtained. Finally, the micro-aggregates self-assemble into the hexagonal plates-shaped $CaCO_3$ microparticles.

The XRD pattern of as-prepared hybrid materials (Fig. 4a) shows that the as-prepared products are composed of pure vaterite phase (JCPDS card no. 01-072-0506). The XRD pattern of the synthesized $CaCO_3$ without the additive-maltose showed the samples was calcite phase [30,32]. This indicates that the maltose play a role on

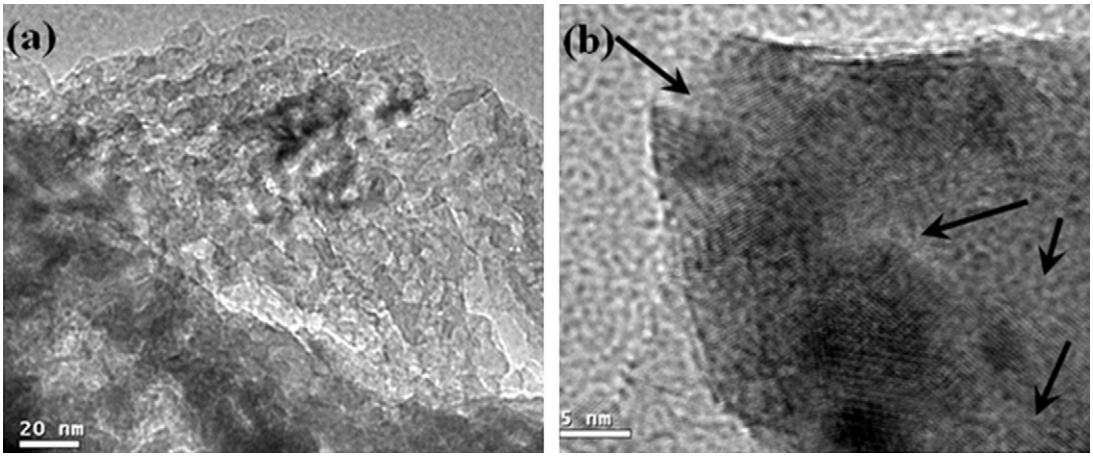

Fig. 2. The TEM (a) and HRTEM (b) images of the obtained hybrid materials.

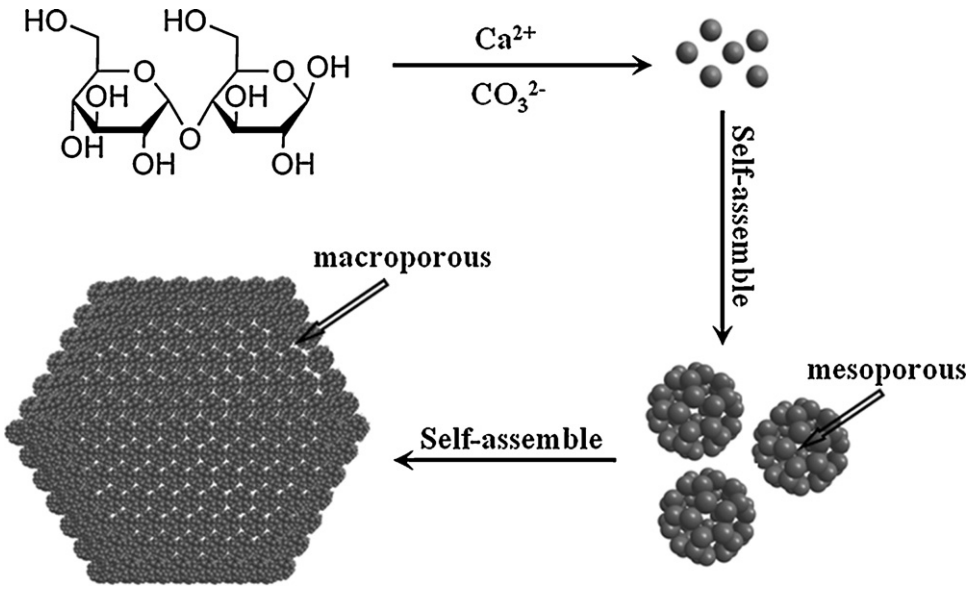

Fig. 3. The formation mechanism of $CaCO_3$–maltose hybrid materials with hierarchical meso/macroporous structure.

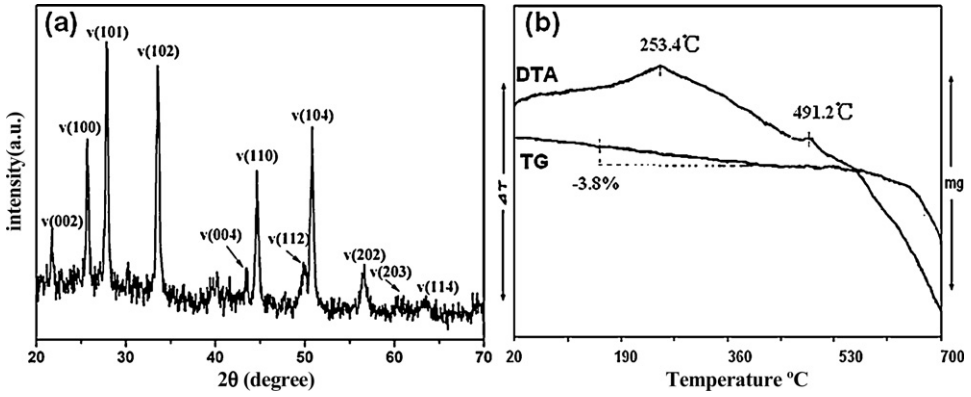

Fig. 4. XRD pattern and TG-DTA curves of the as-prepared $CaCO_3$ crystals.

the formation of the meso/macroporous $CaCO_3$–maltose hybrid materials. Fig. 4b shows the TG-DTA profiles of the synthesized products. The TGA curve of as-prepared $CaCO_3$ demonstrates initial weight loss of 3.8% from 190 to 575 °C, accompanied with two exothermic peaks at around 253 °C and 491.2 °C in the DSC curve, which may be assigned to the decomposition of the intercalated water and organic species. It might indicate that the $CaCO_3$–maltose hybrid materials have been synthesized.

The nitrogen adsorption–desorption isotherms of the synthesized samples and their corresponding pore width distributions are shown in Fig. 5. The N_2 isotherm of the $CaCO_3$–maltose hybrid materials is a type II isotherm (Fig. 5a), indicating that a macroporous structure, with good pore connectivity, may exist in the samples. The nitrogen amount adsorbed rises very steeply at high relative pressure ($P/P_0 > 0.85$), which suggests the presence of an appreciable amount of secondary porosity of very large pores

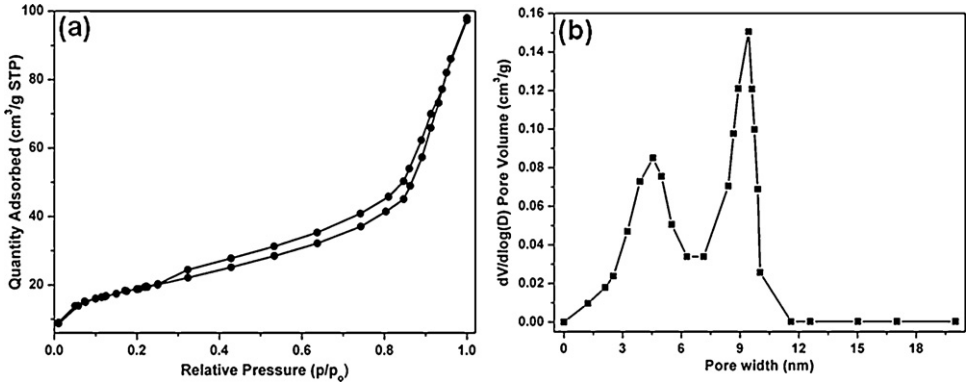

Fig. 5. (a) N_2 adsorption and desorption isotherms and the corresponding BJH pore size distribution curve for the synthesized products.

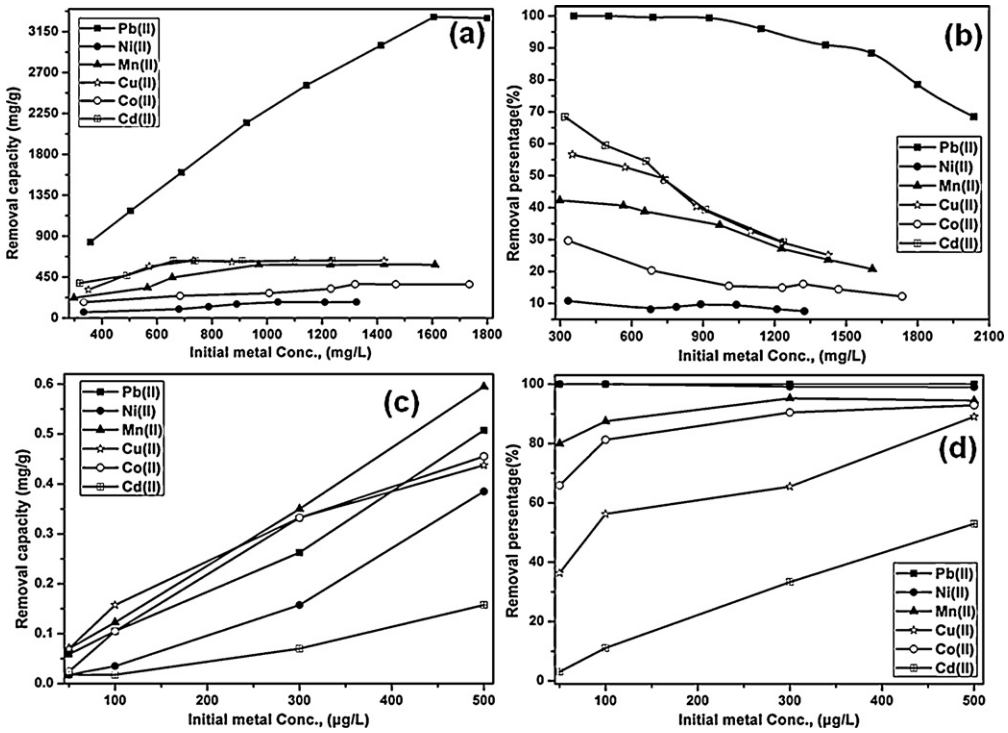

Fig. 6. Effect of initial concentrations of heavy metal solutions (with a pH value of 7) on removal of heavy metals by the $CaCO_3$–maltose hybrid materials.

macropores [11–13]. The isotherms of the hybrid samples exhibited type H3 hysteresis loop that does not exhibit any limiting adsorption at high P/P_0, indicating the hybrid materials consisted of aggregates of plate-like particles giving rise to slit-shaped pores [33]. The pore size distribution curve derived from the adsorption branch of the isotherms shows one broad peak in the range of 2–6 nm, centered at 4.3 nm, and one narrow distribution at 7.5–10 nm (see Fig. 5b). This porosity should be as a result of the organized aggregation of $CaCO_3$ nanoparticles. It indicates that the synthesis in the presence of maltose could efficiently result in the improvement of porosity and textural property of the resultant $CaCO_3$ samples. The BET surface area is 63.2 m^2/g.

3.2. The adsorption of heavy metal ions by $CaCO_3$–maltose hybrid materials

3.2.1. Effect of initial concentration of heavy metal

The effect of initial concentration on the capacity and percentage removal of heavy metals by the $CaCO_3$–maltose hybrid materials is shown in Fig. 6. As Fig. 6a shown, while the dosage of $CaCO_3$–maltose hybrid materials remains constant (0.43 g/L), the removal capacity increases with the increasing initial concentrations of the heavy metal ions till the metals ions uptake value reached the state of equilibrium saturation. Furthermore, it can be observed that the uptake capacity for Pb(II) ions was significantly higher than the other metal ions evaluated. From Fig. 6b, it can be seen that the percentage removal decreases with the increase in initial heavy metal concentration. The percentage removal of Pb^{2+} is almost complete (nearly 100%) at the initial metal ions concentration range 300–900 mg/L for 0.43 g/L adsorbent dose, at pH 7 and a contact time of 5 h. For Mn^{2+}, Ni^{2+}, Cu^{2+}, Co^{2+} and Cd^{2+} at same adsorbent dose and contact time, there are varying degrees of drop in percentage removal at higher initial concentration. It could be attributed to the high collision efficiency between the metal ions and the adsorbent at lower initial metal ion concentrations. However, the metal ions biosorption capacities are no longer enhanced and remain almost constant after saturation at higher concentrations. This may be due to the lack of available sites for adsorbing metal ions on the biosorbents surfaces preventing further adsorption of metal ions [34]. Hence, the percent removal of heavy metals depends on the initial metal ions concentration and decreases with increase in initial metal ions concentration. The difference in percentage removal of different heavy metal ions at the same experimental conditions may be attributed to the difference in the solubility products of their carbonates, chemical affinity and ion exchange capacity with respect to the chemical functional group on the surface of the hybrid materials.

The determination of trace metal ions is required in pollution and toxicological studies because some elements might degrade the quality of water even if present at very low concentrations [35]. It is well known that the trace amounts of metal ions are difficult to remove in solution chemistry. Fig. 6c shows that the removal capacities of these heavy metal ions increases with the increasing initial concentration of these heavy metals from 5 to 500 μg/L. From Fig. 6d, the percentage removal of Pb(II) and Ni(II) are almost complete (nearly 100%) throughout the initial metal ions concentration range. However, contrary to the high concentrations, the removal percentage decreased as the low concentration of heavy metal ions decreased. These results demonstrate that it is not easy to remove trace amounts of metal ions in the solution, but the $CaCO_3$–maltose hybrid materials have the abilities to remove trace metal ions to a large degree.

3.2.2. Effect of contact time

Fig. 7a shows the variation in the percentage removal of the heavy metals with contact time using 0.43 g/L of the $CaCO_3$–maltose hybrid materials and 1000 mg/L of the heavy metal ions at initial pH 7. It is observed that the balance can be established in a short time about 40 min for removal of the above heavy metal ions. Furthermore, for Pb^{2+} ion, the percentage removal is nearly 100% after 30 min. The fast heavy metal ions uptake indicates a high complexation rate between the metal ions and the organic groups

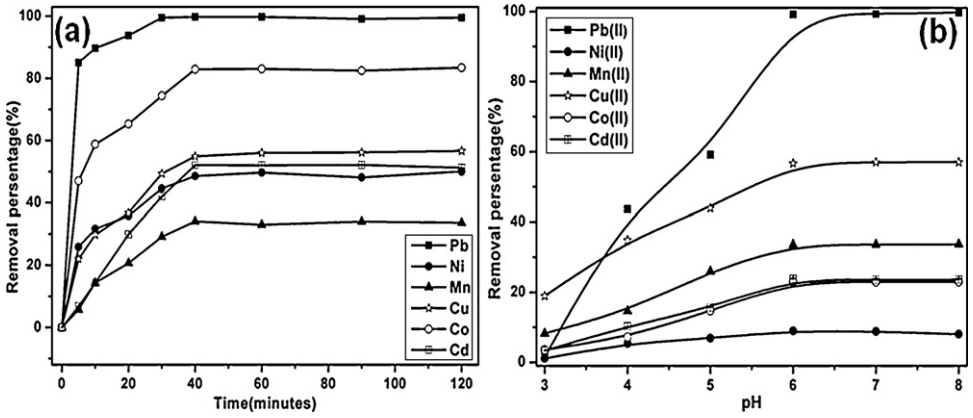

Fig. 7. (a) Effect of contact time and (b) pH values on removal of heavy metal ions by the as-prepared calcium carbonate samples.

in the adsorbent, which is related to their small primary crystallite size of adsorbent and specific surface areas, meso/macroporous structure. The optimal contact time to attain equilibrium with the $CaCO_3$–maltose hybrid materials was experimentally found to be about 1 h. It is evident from the results that the hybrid materials show powerful capability for fast removal of toxic heavy metal ions.

3.2.3. Effect of pH

Fig. 7b shows the effect of pH on heavy metal ions removal efficiencies of the hybrid materials. The removal percentages of these heavy metal ions are found to increase with pH to attain a maximum at pH 6 and thereafter it doesn't change very much with further increase in pH. The maximum removal of Pb^{2+}, Mn^{2+}, Cu^{2+} at pH 7 were found to be nearly 99.7%, 35.8%, 58.8%, respectively, whereas, for Co^{2+}, Cd^{2+} and Ni^{2+} 23.5%, 23.1% and 10% removal at pH 6. From the result, it can be found that the maximum removal of Pb(II) is greatly high than the other metal ions. When the pH is low, the decontaminating effect becomes low because $CaCO_3$ samples could not exist under the low-pH circumstance. When pH exceeded 6 or 7, metals hydroxides could be formed because the formation of the precipitation of heavy metals hydroxides was related to K_{sp} (Supporting Information, Fig. S1). Thus, the maximum adsorption at pH 6–7 may be attributed to the partial hydrolysis of M^{2+}, resulting in the formation of $M(OH)_2$.

3.3. Adsorption isotherms

The adsorption isotherm can show adsorption capacity at different aqueous equilibrium concentration. Fig. 8 shows adsorption isotherms for heavy metal ions on the $CaCO_3$–maltose hybrid materials at pH 7 and 25 °C. The adsorption process could be described by the Langmuir and the Freundlich isotherms. The Langmuir equation assumes that no further adsorption can take place at that site if a heavy metal ion occupies a site, The Langmuir equation is expressed as follows [36]:

$$q_e = \frac{q_{max} K_L C_e}{1 + K_L C_e} \tag{3}$$

or in the linear from

$$\frac{C_e}{q_e} = \frac{1}{q_{max} K_L} + \frac{C_e}{q_{max}} \tag{4}$$

where C_e is the equilibrium concentration of remaining heavy metal ions in solution (mg/L), q_e is the amount of a metal adsorbed per mass unit of sorbent at equilibrium (mg/g), q_{max} is the amount of adsorbate at complete monolayer coverage (mg/g), and K_L is the Langmuir adsorption constant (L/mg) and related to the free energy of adsorption. The constants q_{max} and K_L can be calculated from the intercepts and the slopes of the linear plots of C_e/q_e versus C_e.

The equilibrium adsorption data follow Langmuir's isotherm, which can be observed from Fig. 8a and Table 1. Table 1 indicates that Langmuir model has a limited application for Mn^{2+} and Co^{2+} sorption with a regression coefficient, $R^2 = 0.983$ and 0.920, respectively. A better description for Ni^{2+}, Cu^{2+} and Cd^{2+} sorption data was evident ($R^2 = 0.981$, 0.995 and 0.988). The best fit to the Langmuir model was obtained for Pb^{2+} adsorption, with a correlation coefficient, $R^2 = 0.999$. The maximum sorption capacities for Pb^{2+}, Cd^{2+}, Cu^{2+}, Co^{2+}, Mn^{2+} and Ni^{2+} ions were estimated using the Langmuir equation and found to be 3242.48, 487.80, 628.93, 393.70, 558.66 and 769.23 mg/g, which are relatively higher compared with the literatures [22,23,37,38].

Langmuir parameters calculated from Eq. (5) are listed in Table 1. The essential characteristics of the Langmuir equation

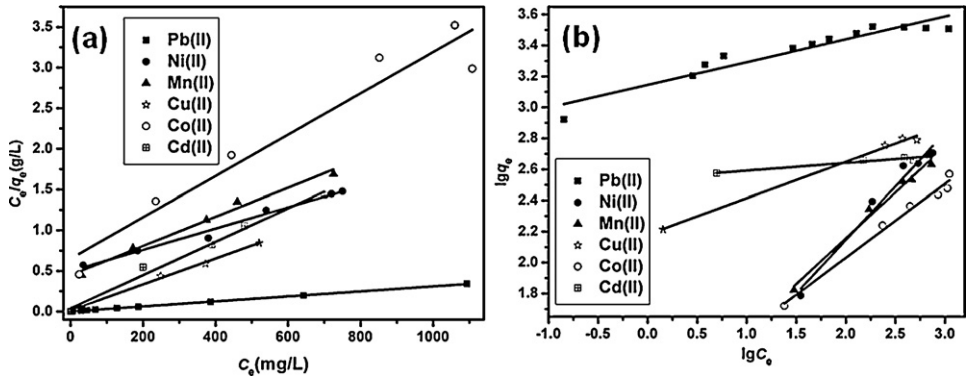

Fig. 8. Langmuir (a) and Freundlich (b) isotherms for metal ions adsorption onto the $CaCO_3$–maltose hybrid materials at 25 °C.

Table 1
Langmuir and Freundlich model parameters.

Metal ions (II)	Langmuir constants				Freundlich constants		
	q_{max} (mg/g)	K_L (L/mg)	R^2	R_L	K_F (mg/g)(L/mg)$^{1/n}$	n	R^2
Pb	3242.48	0.23	0.999	0.004	1396.72	6.80	0.901
Ni	769.23	0.003	0.981	0.243	5.84	1.45	0.969
Mn	558.66	0.004	0.983	0.205	9.42	1.69	0.986
Cu	628.93	0.10	0.995	0.011	151.47	4.27	0.993
Co	393.70	0.004	0.920	0.159	11.94	2.09	0.982
Cd	487.80	0.05	0.988	0.019	348.76	20.22	0.920

can be expressed in term of a dimensionless separation factor, R_L, defined as follows [39]:

$$R_L = \frac{1}{1 + K_L C_0} \quad (5)$$

where C_0 is the highest initial solute concentration and K_L is the Langmuir's adsorption constant (L/mg). From Table 1, it can be found the values of R_L were in the range of 0–1, confirming the favorable uptake of these heavy metal ions.

The Freundlich equation is an empirical equation and has the following form [40]:

$$q_e = K_F C_e{}^{1/n} \quad (6)$$

or in the linear from

$$\ln\ q_e = \ln K_F + \frac{1}{n} \ln C_e \quad (7)$$

where q_e is the solid phase adsorbate concentration in equilibrium (mg/g), C_e the equilibrium liquid phase concentration (mg/L), K_F the Freundlich constant (mg/g)(L/mg)$^{1/n}$ and $1/n$ is the heterogeneity factor. A plot of $\ln q_e$ versus $\ln C_e$ (Fig. 8b) enables the constant K_F and exponent $1/n$ to be determined.

Table 1 indicates that there is a slight deviation from linearity using the Freundlich isotherm model for describing Ni^{2+}, Cu^{2+} and Cd^{2+} sorption. The model gives a poor presentation for Pb^{2+} sorption behavior (R^2 = 0.901). A relatively slight slope $n \gg 1$ indicates that sorption intensity is good over the entire range of concentrations studied, while a steep slope ($n < 1$) means that sorption intensity is good only at high concentrations but much less at lower concentrations [41,42]. It is clear from Table 1 that n values are all greater than 1, indicating that sorption intensity is good over the entire range of concentrations studied. In particular, the n value for Cd^{2+} adsorption is 20.22, which indicates a highly favorable sorption process [42,43].

Table 2 lists the comparison of maximum monolayer adsorption capacity of heavy metal ions onto various adsorbents. Compared with some data obtained from the literatures, the hierarchical meso/macroporous prepared in this work have a relatively large adsorption capacity. In addition, the adsorption of heavy metals by bare $CaCO_3$ had also been determined. Bare $CaCO_3$ could be obtained in the double-distilled water without maltose using the same simple gas-diffusion method. The crystals formed in distilled water were irregular and loose lumps without the macroporous structure of mesoporous framework (Supporting Information, Fig. S2). The adsorption capacity and efficiency of bare $CaCO_3$ for Pb^{2+} was only 62.5 mg/g and 3.77%, respectively. The result indicates that the adsorption capacity and efficiency of bare $CaCO_3$ is very lower than the adsorption capacity and efficiency of $CaCO_3$–maltose hybrids at the same experimental condition. We suggest that there are two possible reasons for the low adsorption capacity and efficiency of bare $CaCO_3$. First, the precipitation transformation mechanism can mainly be considered due to the larger solubility product of $CaCO_3$. However, the adsorption of heavy metals only occur on the surface of the bare $CaCO_3$ without the macroporous structure of mesoporous framework and the heavy metal ions can not further be adsorbed into the interior of bare $CaCO_3$. Second, there are no rich organic ligands in bare $CaCO_3$.

3.4. Interaction of metals with the $CaCO_3$–maltose hybrid materials

The studied heavy metal ions have many different basic properties and the differences between metal sorption capacities may be due to their different affinity to the surface of the $CaCO_3$–maltose hybrid materials. The following rules can be considered as guidelines to consider metal sorption on the $CaCO_3$–maltose surface: (a) ionic radius of M^{2+} cations; metals of ionic radius close to that of Ca^{2+} adsorb stronger than other metals; this rule can explain the higher capacity of Cd^{2+}, Pb^{2+} and Mn^{2+} compared to Co^{2+}. The ionic radius for Co^{2+} is much smaller than Ca^{2+}, while the ionic radii of Cd^{2+}, Pb^{2+} and Mn^{2+} are much closer to that of Ca^{2+} (Table 3). (b) Electronegativity of metals; this rule states that metals of higher electronegativity should adsorb more easily [44]. It can be observed where Pb^{2+}, Ni^{2+} and Cu^{2+} show a higher adsorptive capacity than Co^{2+}, Cd^{2+} and Mn^{2+} and the result is in agreement with this rule. However, Mn^{2+} shows a higher adsorptive capacity than Co^{2+} and Cd^{2+}, which possesses greater electronegativities (Table 3). (c) Solubility of the hydrate complexes; the sorption theory suggested that metals of less soluble complexes with hydrate have increased adsorptive capacity. However, Cu(II) adsorbed less than Pb(II) and Ni(II) which form more soluble hydrate complexes compared to Cu(II) (Table 3). (d) Solubility of the carbonate complexes; the theory suggested that metals that form less soluble complexes with carbonate adsorb stronger than metals which form more soluble complexes. The rule can explain the preferential sorption of Pb^{2+} compared to Cu^{2+}, Co^{2+}, Cd^{2+} and Mn^{2+}, which has lower solubility product

Table 2
Comparison of the maximum monolayer adsorption of the studied metal ions onto the various adsorbents.

Adsorbents	Maximum monolayer adsorption capacity (mg/g)						Reference
	Pb(II)	Ni(II)	Mn(II)	Cu(II)	Co(II)	Cd(II)	
Hierarchical $CaCO_3$–maltose	3242.48	769.23	558.66	628.93	393.70	487.80	This work
Amorphous calcium carbonate	1028.21	537.2				514.62	[22]
Natural calcite	19.92					18.52	[23]
Limestone	0.0167	0.0380		0.0145		0.0184	[43]
Natural Jordanian sorbent	66.2				4.5		[25]
Bare $CaCO_3$	62.5						The control experiment

Table 3
Basic properties of the studied heavy metal ions.

Metal ions(II)	Ionic radius (pm)	Electronegativity (Pauling)	K_{sp} for MCO_3	K_{sp} for $M(OH)_2$
Pb	120	2.33	3.3×10^{-14}	1.4×10^{-20}
Ni	69	1.91	1.4×10^{-17}	5.5×10^{-16}
Mn	80	1.55	2.2×10^{-11}	1.9×10^{-18}
Cu	72	1.90	1.4×10^{-10}	4.8×10^{-20}
Co	72	1.88	1.0×10^{-10}	1.6×10^{-15}
Cd	99	1.69	1.0×10^{-12}	5.3×10^{-15}
Ca	100	1.00	3.4×10^{-9}	5.5×10^{-6}

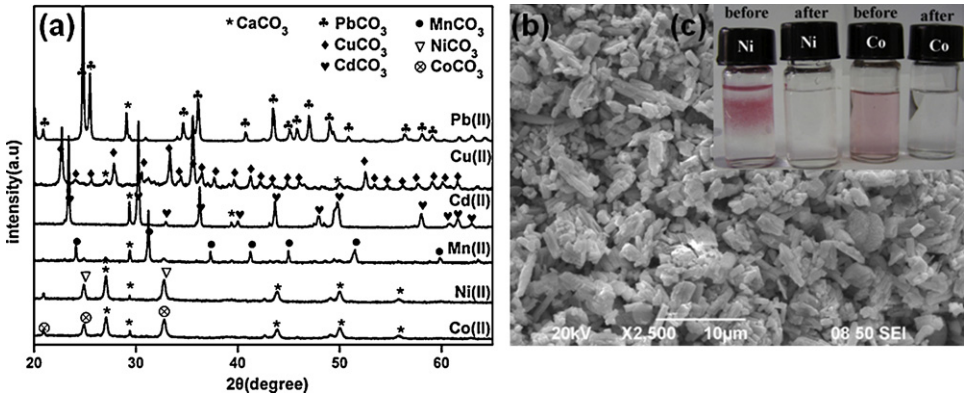

Fig. 9. (a) XRD patterns of precipitates after adsorption with the $CaCO_3$–maltose hybrid materials. Color change before and after removal process by indicators. (b) SEM image of sediments collected after water containing Pb(II) treatment with the $CaCO_3$–maltose hybrid materials. (c) Before and after adsorption with the $CaCO_3$–maltose hybrid materials for Ni^{2+} indicated by dimethylglyoxime solutions and Co^{2+}. (For interpretation of the references to color in this figure legend, the reader is referred to the web version of the article.)

constants. However, the reverse of this rule was also observed in this study. According to this rule, Ni^{2+} should have the highest adsorption capacity of the metals studied. But Ni^{2+} adsorbed less than Pb^{2+}, which has greater solubility product constant in this study (Table 3). Thus, these adsorption capacities of the metal ions are not determined by one of the above rules, but correlates with all the rules. Otherwise, the nature of the adsorbent is also one of the factors, which determines the adsorption capacities of the metal ions.

3.5. Mechanisms of metals sorption

The adsorption mechanism can be considered because of the rich C=O and OH groups of the $CaCO_3$–maltose hybrid materials, which could lead to more effectively coordination with heavy metals. However, the large adsorption capacities of the heavy metal ions indicate that the mechanism of the $CaCO_3$–maltose hybrid materials on removal of heavy metal ions is not through a simple adsorption process. Precipitation transformation must also be

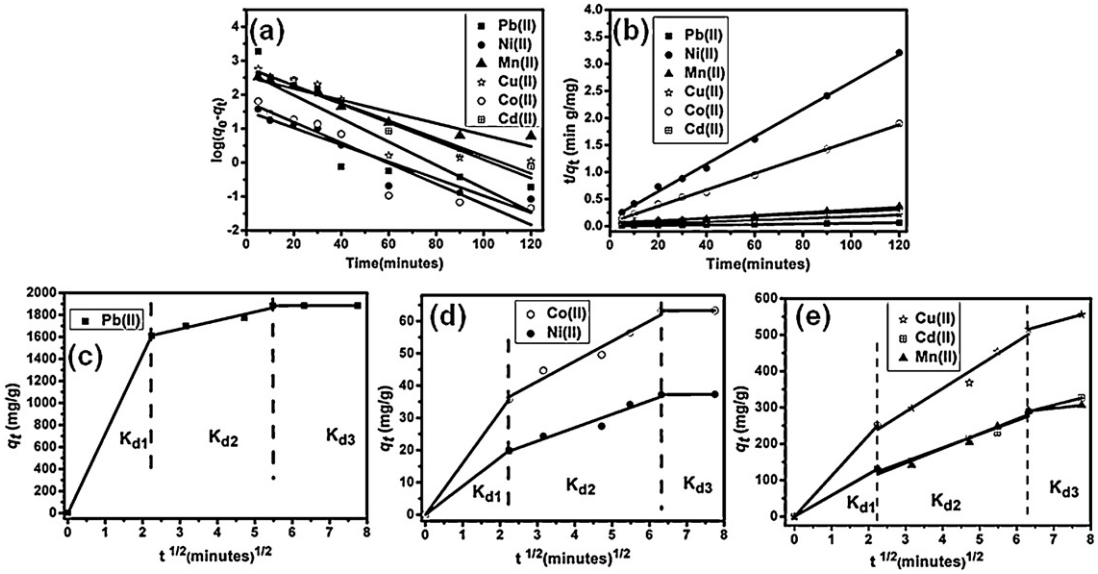

Fig. 10. Pseudo-first-order kinetics (a), second-order kinetics (b) and intra-particle diffusion kinetics (c, d, e) for adsorption of heavy metal ions onto the $CaCO_3$–maltose hybrid materials with hierarchical meso/macroporous structure ($T = 25\,^{\circ}C$; adsorbent dose = 0.43 g/L; pH value = 7).

Table 4
Pseudo-first-order adsorption kinetic constants of the $CaCO_3$–maltose hybrid material.

Metal ions(II)	C_0 (mg/L)	$q_{e,exp}$ (mg/g)	Pseudo-first-order model		
			$q_{e,cal}$ (mg/g)	K_1 ($\times 10^{-3}$ min^{-1})	R^2
Pb	811.5	1884.2	469.16	79.04	0.73
Ni	43.8	37.4	33.18	57.48	0.89
Mn	565.2	332.5	330.58	39.22	0.90
Cu	572.4	566.9	644.08	62.59	0.84
Co	43.4	63.5	62.02	69.55	0.87
Cd	410.1	367.5	610.46	59.69	0.92

Table 5
Pseudo-second-order adsorption kinetic constants of the $CaCO_3$–maltose hybrid material.

Metal ions(II)	C_0 (mg/L)	$q_{e,exp}$ (mg/g)	Pseudo-second-order model		
			$q_{e,cal}$ (mg/g)	K_2 ($\times 10^{-4}$ g/mg min^{-1})	R^2
Pb	811.5	1884.2	1901	6.17	0.99
Ni	43.8	37.4	39.5	47.03	0.99
Mn	565.2	332.5	397.1	1.40	0.97
Cu	572.4	566.9	621.2	1.79	0.99
Co	43.4	63.5	66.4	33.33	0.99
Cd	410.1	367.5	485.4	0.73	0.96

considered. This solubility product of $CaCO_3$ is relatively larger than the studied metal carbonates, which should definitely promote transformation of precipitation between $CaCO_3$ and heavy metal carbonates. The phase of precipitates after treatment was determined by XRD (as Fig. 9a shown). From the results, the precipitates consist mainly of studied metal carbonate, which indicates that the $CaCO_3$ could be transformed after being stirred for 2 h in the metal ions solution. Moreover, the morphology of precipitates collected had been changed, which shows that a recrystallization process occurred in such water treatment process (Fig. 9b).

To make the decontamination effect of the $CaCO_3$–maltose hybrid materials visually, coordination complex (dimethylglyoxime) was used as indicators. Fig. 9c reveals that the concentration of Ni^{2+} ion in the aqueous solution decreased dramatically after absorption with as-obtained samples. The Ni^{2+} solution after absorption by the $CaCO_3$–maltose hybrid materials shows no color change with the addition of dimethylglyoxime, indicating almost complete removal of Ni^{2+} ion. So does Co^{2+} ion, the color of Co^{2+} appear after adsorption by the $CaCO_3$–maltose hybrid materials.

3.6. Adsorption kinetics

Three known kinetic models are used to investigate the mechanism of the adsorption [45,46]. Firstly, pseudo-first-order equation has been widely used for analyzing the adsorption of an adsorbate from an aqueous solution.

$$\log(q_e - q_t) = \log q_e - \frac{tk_1}{2.303} \quad (8)$$

where q_e and q_t are the amounts of heavy metal ions adsorbed (mg/g) at equilibrium and at time t (min), respectively, and k_1 (min^{-1}) is the rate constant adsorption. Values of k_1 are calculated from the plots of $\log(q_e - q_t)$ versus t (see Fig. 10a) for the $CaCO_3$–maltose hybrid materials. The R^2 values obtained are relatively small and the experimental q_e values do not agree with the calculated values obtained from the linear plots (Table 4).

Secondly, the pseudo-second-order equation based on equilibrium adsorption also has been widely used for analyzing the adsorption of an adsorbate from an aqueous solution:

$$\frac{t}{q_t} = \frac{1}{k_2 q_e^2} + \frac{t}{q_e} \quad (9)$$

where k_2 (g/mg min) is the rate constant of second-order adsorption. The linear plot of t/q_t versus t is shown in Fig. 10b and the obtained R^2 values are greater than 0.96 for all samples. It indicates a good agreement between the experimental and the calculated q_e values (Table 5), showing the applicability of above equation for the $CaCO_3$–maltose hybrid materials.

Only the above two kinetic models were not enough to explain the diffusion mechanism, thus intra-particle diffusion kinetic model based on the theory or equation proposed by Weber and Morris is tested [47]. The kinetic model is an empirically functional relationship, common to the most adsorption processes. The adsorbate uptake varies almost proportionally with $t^{1/2}$. According to the following Weber–Morris's equation:

$$q_t = k_{di}\sqrt{t} + c_i \quad (10)$$

where k_{di} is the rate parameter of stage i (mg/g h$^{1/2}$), calculated from the slope of the straight line of q_t versus $t^{1/2}$. C_i is the intercept of stage i, giving an idea about the thickness of boundary layer. That is to say, the larger the intercept indicates the greater the boundary layer effect.

Fig. 10c and d presents a linear fit of intra-particle diffusion model for adsorption of heavy metal ions onto the $CaCO_3$–maltose

Table 6
Intra-particle diffusion model constants and correlation coefficients for adsorption of metal ions on the $CaCO_3$–maltose hybrid material.

Metal ions	C_0 (mg/L)	Intra-particle diffusion model								
		K_{d1} (mg/g min$^{1/2}$)	K_{d2} (mg/g min$^{1/2}$)	K_{d3} (mg/g min$^{1/2}$)	C_1	C_2	C_3	$(R_1)^2$	$(R_2)^2$	$(R_3)^2$
Pb	811.5	718.68	77.74	0.16	0	1438.36	1882.59	1.00	0.95	1.00
Ni	43.8	8.86	4.16	0.05	0	10.34	36.87	1.00	0.94	1.00
Mn	565.2	58.11	40.34	11.12	0	25.99	220.02	1.00	0.96	1.00
Cu	572.4	111.71	64.27	28.11	0	95.35	337.69	1.00	0.96	1.00
Co	43.4	15.95	6.25	0.03	0	22.52	63.07	1.00	0.96	1.00
Cd	410.1	58.55	37.35	25.80	0	39.92	125.86	1.00	0.96	1.00

hybrid materials. From the results, it can be observed that such types of plots present multilinearity, indicating that three steps take place. First, sharper region is the instantaneous adsorption or external surface adsorption stage, which was completed within the first 5 min. The possible reason could be that the high initial heavy metal ion concentration is driving force of diffusion. Second, the region is the gradual adsorption stage where intra-particle diffusion is the rate limiting step. It can be speculated that the precipitation transformation happened in this process. Then, the third region is the final equilibrium stage where intra-particle diffusion further slows down because of the low concentrations of heavy metal ions left in the solutions [45]. It is clearly that the rate of external surface adsorption (stage 1) of Pb(II) is higher than that the other ions with the $CaCO_3$–maltose (Table 6). As discussed above, heavy metal ions are slowly transported via intra-particle diffusion into macroporous and are finally retained in hierarchical mesoporous. The rate parameters for Pb(II) show that the value of k_{d1} and k_{d2} is larger than that the other metal ions. We speculated that the reason could be the lager chemical affinity and the smallest solubility products of $PbCO_3$. Further observation indicates $k_{d1} > k_{d2} > k_{d3}$. This is easy to understand because the concentration of metal ions left in the solutions gradually decreases.

4. Conclusion

The $CaCO_3$–maltose hybrid materials with hierarchical meso/macroporous structure have been successfully prepared in the presence of maltose under a simple evaporation diffusion method. The $CaCO_3$–maltose hybrid materials is found to be effective and alternative adsorbent for the removal of heavy metal ions from wastewater as a result of hierarchical meso/macroporous structure, rich organic ligands of the $CaCO_3$–maltose hybrid materials and the larger solubility product of $CaCO_3$.

Acknowledgments

This work was financially supported by the National Science Foundation of China (Grant Nos. 21171051 and 20871042), the Innovation Scientists and Technicians Troop Construction Projects of Henan Province (Grant No. 114200510004) and Program for Chang jiang Scholars and Innovative Research Team in University (Grant No. IRT 1061).

Appendix A. Supplementary data

Supplementary data associated with this article can be found, in the online version, at doi:10.1016/j.jhazmat.2012.01.054.

References

[1] R.P. Schwarzenbach, B.I. Escher, K. Fenner, T.B. Hofstetter, C.A. Johnson, U. Gunten, B. Wehrli, The challenge of micropollutants in aquatic systems, Science 313 (2006) 1072–1077.
[2] D.R. Baldwin, W.J. Marshall, Heavy metal poisoning and its laboratory investigation, Ann. Clin. Biochem. 36 (1999) 267–300.
[3] D. Mohan, K.P. Singh, Single- and multi-component adsorption of cadmium and zinc using activated carbon derived from bagasse – an agricultural waste, Water Res. 36 (9) (2002) 2304–2318.
[4] X.M. Zhao, D.M. Dong, X.Y. Hua, S.F. Dong, Investigation of the transport and fate of Pb, Cd, Cr(VI) and As(V) in soil zones derived from moderately contaminated farmland in Northeast, China, J. Hazard. Mater. 170 (2009) 570–577.
[5] S. Dai, M.C. Burleigh, Y.H. Ju, H.J. Gao, S. Lin, S.J. Pennycook, C.E. Barnes, Z.L. Xue, Hierarchically imprinted sorbents for the separation of metal ions, J. Am. Chem. Soc. 122 (5) (2000) 992–993.
[6] V. Antochshuk, M. Jaroniec, 1-Allyl-3-propylthiourea modified mesoporous silica for mercury removal, Chem. Commun. (2002) 258–259.
[7] S.Z. Qiao, H. Djojoputro, Q.H. Hu, G.Q. Lu, Synthesis and lysozyme adsorption of rod-like large-pore periodic mesoporous organosilica, Prog. Solid State Chem. 34 (2006) 249–256.
[8] A. Vinu, V. Murugesan, M. Hartmann, Adsorption of lysozyme over mesoporous molecular sieves MCM-41 and SBA-15: influence of pH and aluminum incorporation, J. Phys. Chem. B 108 (22) (2004) 7323–7330.
[9] S. Dai, M.C. Burleigh, Y. Shin, C.C. Morrow, C.E. Barnes, Z. Xue, Imprint coating: a novel synthesis of selective functionalized ordered mesoporous sorbents, Angew. Chem. Int. Ed. 38 (1999) 1235–1239.
[10] L. Mercier, T.J. Pinnavaia, Heavy metal ion adsorbents formed by the grafting of a thiol functionality to mesoporous silica molecular sieves: factors affecting Hg(II) uptake, Environ. Sci. Technol. 32 (1998) 2749–2754.
[11] R.C. Schroden, M. Al-Daous, S. Sokolov, B.J. Melde, J.C. Lytle, A. Stein, M.C. Caubajo, J.T. Fernàndez, E.E. Rodrìguez, Hybrid macroporous materials for heavy metal ion adsorption, J. Mater. Chem. 12 (2002) 3261–3267.
[12] X.J. Zhang, T.Y. Ma, Z.Y. Yuan, Titania–phosphonate hybrid porous materials: preparation, photocatalytic activity and heavy metal ion adsorption, J. Mater. Chem. 18 (17) (2008) 2003–2010.
[13] A.M. Liu, K. Hidajat, S. Kawi, D.Y. Zhao, A new class of hybrid mesoporous materials with functionalized organic monolayers for selective adsorption of heavy metal ions, Chem. Commun. (2000) 1145–1146.
[14] J. Brown, L. Mercier, T.J. Pinnavaia, Selective adsorption of Hg^{2+} by thiol-functionalized nanoporous silica, Chem. Commun. (1999) 69–70.
[15] Z.Y. Yuan, B.L. Su, Insights into hierarchically meso–macroporous structured materials, J. Mater. Chem. 16 (2006) 663–677.
[16] T.Y. Ma, X.J. Zhang, G.S. Shao, J.L. Cao, Z.Y. Yuan, Ordered macroporous titanium phosphonate materials: synthesis, photocatalytic activity, and heavy metal ion adsorption, J. Phys. Chem. C 112 (2008) 3090–3096.
[17] T.Y. Ma, X.J. Zhang, Z.Y. Yuan, Hierarchical meso-/macroporous aluminum phosphonate hybrid materials as multifunctional adsorbents, J. Phys. Chem. C 113 (2009) 12854–12862.
[18] T.Y. Ma, X.J. Zhang, Z.Y. Yuan, Hierarchically meso-/macroporous titanium tetraphosphonate materials: synthesis, photocatalytic activity and heavy metal ion adsorption, Micropor. Mesopor. Mater. 123 (2009) 234–242.
[19] T.Y. Ma, X.J. Zhang, Z.Y. Yuan, High selectivity for metal ion adsorption: phosphonated titanias to meso-/macroporous phosphonates, J. Mater. Sci. 44 (2009) 6775–6785.
[20] X.Z. Lin, T.Y. Ma, Z.Y. Yuan, Titania-silica-phosphonate triconstituent hybrid mesoporous materials as adsorbents in gas and liquid phases, Chem. Eng. J. 166 (2011) 1144–1151.
[21] X.M. Ma, H.F. Chen, L. Yang, K. Wang, Y.M. Guo, L. Yuan, Construction, potential applications of a functionalized cell with an intracellular mineral scaffold, Angew. Chem. Int. Ed. 50 (2011) 7414–7417.
[22] G.B. Cai, G.X. Zhao, X.K. Wang, S.H. Yu, Synthesis of polyacrylic acid stabilized amorphous calcium carbonate nanoparticles and their application for removal of toxic heavy metal Ions in water, J. Phys. Chem. C 114 (30) (2010) 12948–12954.
[23] Ö. Yavuz, R. Guzel, F. Aydin, I. Tegin, R. Ziyadanogullari, Removal of cadmium and lead from aqueous solution by calcite, Pol. J. Environ. Stud. 16 (3) (2007) 467–471.
[24] S.L. Stipp, M.F. Hochella, J.G.A. Parks, J.O. Leckie, Cd^{2+} uptake by calcite, solid-state diffusion, and the formation of solid-solution: interface processes observed with near-surface sensitive techniques (XPS, LEED, and AES), Geochim. Cosmochim. Acta 56 (1992) 1941–1954.
[25] Y.S. Al-Degs, M.I. El-Barghouthi, A.A. Issa, M.A. Khraisheh, G.M. Walker, Sorption of Zn(II), Pb(II), and Co(II) using natural sorbents: equilibrium and kinetic studies, Water Res. 40 (2006) 2645–2658.
[26] M. Shirvani, M. Kalbasi, H. Shariatmadari, F. Nourbakhsh, B. Najafi, Sorption–desorption of cadmium in aqueous palygorskite, sepiolite, and calcite suspensions: isotherm hysteresis, Chemosphere 65 (2006) 2178–2184.
[27] D.V. Leff, L. Brandt, J.R. Heath, Synthesis and characterization of hydrophobic, organically-soluble gold nanocrystals functionalized with primary amines, Langmuir 12 (1996) 4723–4730.
[28] C.D. Keating, K.M. Kovaleski, M.J. Natan, Protein: colloid conjugates for surface enhanced Raman scattering: stability and control of protein orientation, J. Phys. Chem. B 102 (47) (1998) 9404–9413.
[29] C.D. Keating, K.M. Kovaleski, M.J. Natan, Heightened electromagnetic fields between metal nanoparticles: surface enhanced Raman scattering from metal-cytochrome c-metal sandwiches, J. Phys. Chem. B 102 (47) (1998) 9414–9425.
[30] X.M. Ma, L.P. Li, L. Yang, C.Y. Su, Y.M. Guo, K. Jiang, Preparation of highly ordered hierarchical $CaCO_3$ hemisphere and the application as pH value-sensitive anticancer drug carrier, Mater. Lett. 65 (2011) 3176–3179.
[31] X.M. Ma, H.Y. Yang, H.F. Chen, L. Yang, Y.M. Guo, Y.Y. Si, Protein-directed self-assembly of $CaCO_3$ nanoparticles into hierarchical superstructures, J. Cryst. Growth 327 (2011) 146–153.
[32] H.Y. Yang, W.G. Yao, L. Yang, X.M. Ma, H.J. Wang, F. Ye, K.W. Wong, Biomimetic fabrication of alginate/$CaCO_3$ hybrid beads for dual-responsive drug delivery under compressed CO_2, J. Cryst. Growth 311 (2009) 2682–2688.
[33] K.S.W. Sing, Reporting physisorption data for gas/solid systems with special reference to the determination of surface area and porosity, Pure Appl. Chem. 54 (11) (1982) 2201–2222.
[34] A.K. Meena, G.K. Mishra, P.K. Rai, C. Rajagopal, P.N. Nagar, Removal of heavy metal ions from aqueous solutions using carbon aerogel as an adsorbent, J. Hazard. Mater. 122 (2005) 161–170.
[35] W.H.O., Guidelines for Drinking-Water Quality, World Health Organization, Geneva, 2006.
[36] I. Langmuir, Adsorption of gases on plain surfaces of glassmica platinum, J. Am. Chem. Soc. 40 (1918) 1361–1403.

[37] S. Babel, T.A. Kurniawan, Comparative study of the biosorption of Pb(II), Ni(II) and Cr(VI) ions onto *S. cerevisiae*: determination of biosorption heats, J. Hazard. Mater. 97 (2003) 219–229.
[38] A. ÜÇer, A. Uyanik, Ş.F. Aygün, Adsorption of Cu(II), Cd(II), Zn(II), Mn(II) and Fe(III) ions by tannic acid immobilised activated carbon, Sep. Purif. Technol. 47 (2006) 113–118.
[39] K.R. Hall, L.C. Eagleton, A. Acrivos, T. Vermeulen, Pore and solid diffusion kinetics in fixed-bed adsorption under constant pattern conditions, Ind. Eng. Chem. Fundam. 5 (1996) 212–223.
[40] Y.S. Al-Degs, M.I. El-Barghouthi, A.H. El-Sheikh, G.M. Walker, Removal of disperse 2BLN dye from industrial water onto activated carbon prepared from sugar can stalks, Dyes Pigments 77 (1) (2008) 16–23.
[41] F.H. Frimmel, L. Huber, Influence of humic substances on the aquatic sorption of heavy metals on defined minerals phases, Environ. Int. 22 (1996) 507–517.
[42] G. McKay, The removal of color from effluent using various adsorbents-IV silica, Water Res. 14 (1980) 1–27.
[43] H.A. Aziz, M.N. Adlan, K.S. Ariffin, Heavy metals (Cd, Pb, Zn, Ni, Cu and Cr(III)) removal from water in Malaysia: post treatment by high quality limestone, Bioresour. Technol. 99 (2008) 1578–1583.
[44] M.B. McBride, Chemisorption and precipitation of inorganic ions, in: Environmental Chemistry of Soils, Oxford University Press, New York, 1994.
[45] I.A.W. Tan, A.L. Ahmad, B.H. Hameed, Adsorption isotherms, kinetics, thermodynamics and desorption studies of 2,4,6-trichlorophenol on oil palm empty fruit bunch-based activated carbon, J. Hazard. Mater. 164 (2009) 473–482.
[46] Y.S. Ho, G.S. Mckay, Second-order kinetic model for the sorption of cadmium onto tree fern: a comparison of linear and non-linear methods, Water Res. 34 (2000) 735–742.
[47] W.J. Weber, J.C. Morris, Proceedings of the International Conference on Water Pollution Symposium, vol. 2, Pergamon, Oxford, 1962, pp. 231–266.